Resonant Interactions between a Mollow Triplet Sideband and a Strongly Coupled Cavity

Hyochul Kim,[1] Thomas C. Shen,[1] Kaushik Roy-Choudhury,[1] Glenn S. Solomon,[2] and Edo Waks[1,*]
[1]Department of Electrical and Computer Engineering, IREAP, and Joint Quantum Institute, University of Maryland, College Park, Maryland 20742, USA
[2]Joint Quantum Institute, National Institute of Standards and Technology, and University of Maryland, Gaithersburg, Maryland 20899, USA
(Received 9 October 2013; published 8 July 2014)

We demonstrate resonant coupling of a Mollow triplet sideband to an optical cavity in the strong coupling regime. We show that, in this regime, the resonant sideband is strongly enhanced relative to the detuned sideband. Furthermore, the linewidth of the Mollow sidebands exhibits a highly nonlinear pump power dependence when tuned across the cavity resonance due to strong resonant interactions with the cavity mode. We compare our results to calculations using the effective phonon master equation and show that the nonlinear linewidth behavior is caused by strong coherent interaction with the cavity mode that exists only when the Mollow sideband is near cavity resonance.

DOI: 10.1103/PhysRevLett.113.027403 PACS numbers: 78.67.Hc, 42.50.Hz, 78.55.−m, 78.67.De

The resonance fluorescence spectrum of atomic systems is of great interest for studying fundamental properties of light-matter interactions. It also plays an important role in quantum information processing applications as a method for performing nondestructive quantum state readout [1–3], generating single photons [4–6], and creating entangled quantum network nodes [7,8]. When an atomic system is strongly driven, the resonance fluorescence emission exhibits the well-known Mollow triplet spectrum [9], which has been observed using atoms [10] as well as solid-state quantum emitters such as quantum dots [11–16]. The Mollow triplet emission provides a promising approach to generate single and sequential photons [17], as well as light-matter entangled states [14].

Recently, there has been significant interest in understanding the properties of a strongly driven atomic system coupled to a cavity. Cavities can enhance the emission efficiency of resonance fluorescence, leading to brighter photon sources. They also open up the possibility for new applications such as dressed-state lasing [18] that could enable novel quantum optical devices. Furthermore, cavities can provide a better fundamental understanding of coupling between phonons and solid-state quantum emitters such as quantum dots by enhancing their interaction. This enhancement leads to pronounced nonlinear effects such as large power broadening of the Mollow sideband [19–23].

Previous studies of strongly driven quantum dots in a cavity operated in the regime where the Rabi frequency was much smaller than the detuning between the cavity and the emitter. In this regime, the entire resonance fluorescence spectrum of the quantum dot is highly detuned from the cavity. The coherent interaction between the sideband and the cavity is therefore weak, but the quantum dot can still interact incoherently with the cavity through a broad continuum of phonon states. However, many applications of a strongly driven atomic system in a cavity require the large Rabi frequency regime where the sideband is tuned onto or even beyond the cavity resonance. This regime also enables the study of direct resonant interactions between a Mollow sideband and a cavity mode. The large Rabi frequency regime was studied in early work utilizing atomic beams of barium coupled to a large mode-volume Fabry-Perot cavity that served as a tunable photon reservoir [24,25]. Due to the large cavity mode volume, the coupling strength between the atomic beam and the cavity was very weak in these experiments, leading to only a small asymmetry of the Mollow spectrum. Furthermore, no power induced broadening was reported. The large Rabi frequency regime has not yet been demonstrated in a strongly coupled atom-cavity system. In this regime, significant enhancement of the Mollow sideband is expected, and recently theoretical predictions have also shown that it may exhibit unexpected physical properties such as a nonlinear pump power dependence of the Mollow sideband linewidth [26].

In this letter, we report an experimental realization of the large Rabi frequency regime in a strongly coupled atom-cavity system. We use a single InAs quantum dot strongly coupled to a photonic crystal cavity to attain Rabi frequencies exceeding 100 GHz, enabling us to tune a Mollow sideband over the entire resonant spectrum of the cavity. We show that the emission intensity of the cavity-resonant sideband is enhanced relative to detuned sideband by as much as a factor of 6. We also observe a highly nonlinear power dependence of the Mollow triplet sideband linewidths as one of the sidebands is tuned across the cavity mode, consistent with recent theoretical predictions [26]. By comparing our experimental results to calculations based on an effective phonon master equation [23], we show that this nonlinear power dependence is caused by strong

coherent interaction between the cavity and quantum dot. This coherent contribution plays a strong role only when the Mollow sideband is near cavity resonance, in contrast to the small Rabi frequency regime where interactions with the cavity are incoherently mediated by phonons and the linewidth of the Mollow sideband increases linearly with pump power [19,21]. These results provide insight to the emission spectrum of the Mollow sideband in a cavity, and have important implications for the coherence properties of generated single photons as well as the achievable linewidths and thresholds of dressed state lasers.

The system we study is an InAs quantum dot strongly coupled to a GaAs photonic crystal three-hole defect cavity [27]. Figure 1(a) shows a scanning electron microscope image of a fabricated cavity. The sample consists of 160 nm GaAs membrane with a single layer of InAs quantum dots (density of 10–50/μm^2) at the center. The GaAs membrane is grown on top of a 1 μm AlGaAs sacrificial layer. We fabricate photonic crystal cavities using electron beam lithography and chlorine based dry etching, followed by a wet etch of the sacrificial layer to create a membrane.

Figure 1(b) shows the measurement setup. Sample excitation and collection are performed with a confocal microscope using an objective lens with numerical aperture of 0.68. We excite the sample using either a Ti:Sapphire laser emitting at 780 nm for photoluminescence measurements, or with a narrow linewidth (< 300 kHz) tunable diode laser for resonance fluorescence measurements. The collected signal is measured using a grating spectrometer with a resolution of 7 GHz and detected by a charged coupled device (CCD). A cross-polarization setup rejects the component of the excitation laser that does not couple to the cavity mode.

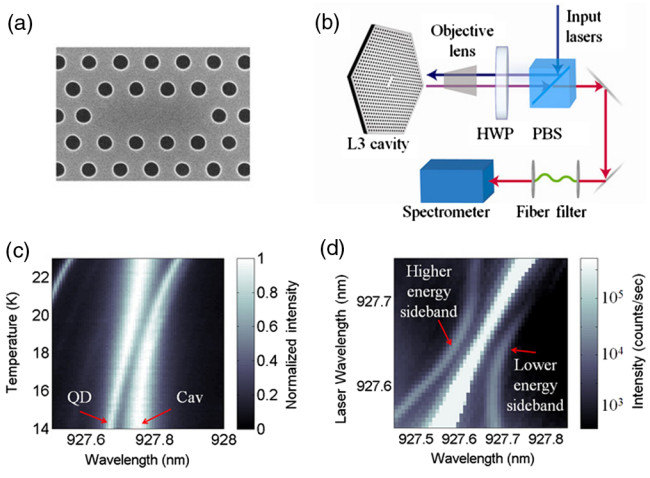

FIG. 1 (color online). (a) Scanning electron microscope image of a fabricated photonic crystal cavity. (b) Schematic of the measurement setup. HWP: half-wave plate, PBS: polarizing beam splitter. (c) Photoluminescence spectra as a function of temperature. (d) Resonance fluorescence spectra when the excitation laser is scanned across the quantum dot resonance at a pump power of 8.0 μW. Along with a strong laser signal, two Mollow triplet sidebands are observed.

For high-resolution spectral measurements, we use a tunable fiber Fabry-Perot filter with 0.9 GHz bandwidth in front of the spectrometer.

We first characterize the device through photoluminescence. Figure 1(c) shows the measured spectrum as a function of the sample temperature. The spectrum shows two resonances, one which corresponds to the direct cavity emission and a second due to a quantum dot. As the sample temperature increases, the quantum dot resonance redshifts and exhibits a clear anticrossing with the cavity, indicating that the system operates in the strong coupling regime. A minimum energy separation (ΔE) of 101 μeV (24.7 GHz) is observed on resonance at 18.5 K. When the quantum dot is detuned from the cavity, the photoluminescence from the bare cavity shows a quality factor of 9100, corresponding to a cavity energy decay rate of $\kappa/2\pi = 36$ GHz. The coupling strength g is calculated to be $g/2\pi = 15.3$ GHz using the relation $\Delta E = 2\hbar\sqrt{g^2 - (\kappa/4)^2}$.

Figure 1(d) shows the resonance fluorescence spectrum taken when the narrow band diode laser is swept over the quantum dot emission wavelength at temperature of 5 K. We set the diode laser power to 8.0 μW and measure the spectrum directly using the spectrometer without the fiber filter. We reject a large fraction of the direct laser scatter from the sample surface using a cross-polarization setup and spatially filtering with a single mode fiber. The cavity mode is blue-detuned from the quantum dot by 0.24 nm and lies outside the plotted wavelength range. When the laser is tuned close to the quantum dot emission line (927.64 nm), the spectrum exhibits a Mollow triplet.

Figure 2(a) shows the resonance fluorescence spectrum as a function of $\sqrt{P}$, where P is the pump power measured before

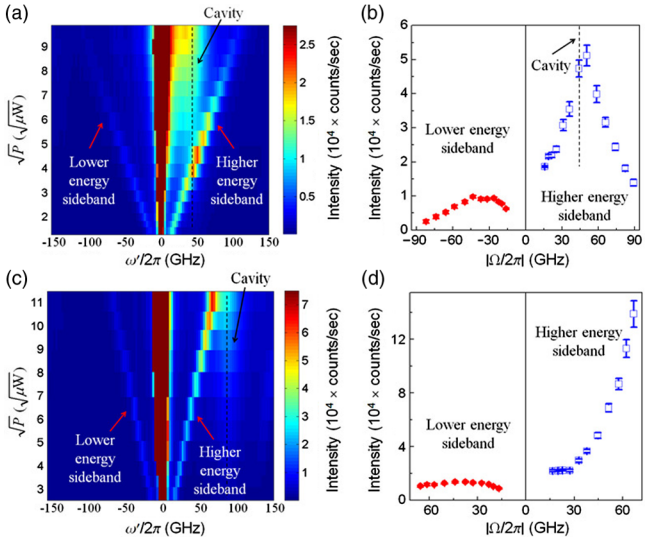

FIG. 2 (color online). (a) Resonance fluorescence spectra of a quantum dot coupled to a photonic crystal cavity as a function of $\sqrt{P}$ for $\Delta_{cx}/2\pi = 42$ GHz. (b) Measured emission intensity of the Mollow triplet sidebands as a function of $\Omega/2\pi$. (c) Same as panel a for $\Delta_{cx}/2\pi = 85$ GHz. (d) Same as panel b for $\Delta_{cx}/2\pi = 85$ GHz.

the objective lens. The x axis is the relative frequency $\omega' = \omega - \omega_L$, where ω is the measured frequency and ω_L is a laser frequency. The detuning between the quantum dot emission frequency (ω_x) and cavity (ω_c) is $\Delta_{cx}/2\pi = (\omega_c - \omega_x)/2\pi = 42$ GHz (0.12 nm), and the excitation laser is tuned to resonance with the quantum dot. At each power, the Mollow triplet sidebands are symmetrically spaced on the longer and shorter wavelength sides of the quantum dot emission and their spectral separation increases linearly with $\sqrt{P}$. The Rabi frequency Ω is related to the splitting between two sidebands, denoted $\Delta\omega$, by $\Omega = 1/2\ \Delta\omega$. At the maximum pump power, we achieve a Rabi frequency exceeding $\Omega/2\pi = 100$ GHz, which is much greater than $\Delta_{cx}/2\pi$. Thus we are able to drive the system both in the small Rabi frequency regime ($\Omega < \Delta_{cx}$) and the large Rabi frequency regime ($\Omega > \Delta_{cx}$).

At a pump power of 13.4 μW, the higher energy sideband is resonant with the cavity mode (black dashed line). We observe a clear enhancement of the higher energy sideband emission intensity under this condition. This enhancement results in a highly asymmetric spectrum where the higher energy sideband is much brighter than the lower energy sideband. At even higher pump power, the higher energy sideband tunes beyond the cavity resonance and is diminished. We note that at very high pump power the bare cavity emission appears in the spectrum. This emission is attributed to phonon induced nonresonant energy transfer of the quantum dot excitation [28–32].

In Fig. 2(b), we plot the emission intensity of the higher (blue open squares) and lower (red full circles) energy sidebands as a function of the Rabi frequency. To determine the Rabi frequency and intensity, we fit the measured spectrum at each laser power to four Lorentzians, one for each sideband, one for the laser scatter, and one for the cavity which is excited by inelastic scattering. When the higher energy sideband is within 10 GHz of the cavity resonance, it becomes difficult to separate it from the cavity emission due to inelastic scattering. In this region, we interpolate the cavity emission using the closest data points outside the 10 GHz window. Figure 2(b) shows a clear resonant behavior where the sideband is enhanced near cavity resonance, resulting in a large emission asymmetry. The higher energy sideband is 6 times brighter than the lower energy sideband at a pump power of 24.6 μW ($\Omega/2\pi = 57.8$ GHz).

Figures 2(c)–2(d) show the spectrum as a function of pump power where the detuning between the cavity and quantum dot is increased to $\Delta_{cx}/2\pi = 85$ GHz (0.24 nm) by gradual gas condensation that occurs naturally in the vacuum chamber [33,34]. Here, the detuning is greater than the maximum achievable Rabi frequency so the system remains in the small Rabi frequency regime for all pump powers. Because of the larger detuning, the Mollow sideband does not cross the cavity resonant frequency and we do not observe a resonance behavior. Instead, the sideband emission intensity gradually increases as it tunes closer to resonance with the cavity.

In addition to the asymmetry and intensity increase, Fig. 2(a) shows indications of linewidth broadening. The sideband linewidth is predicted to exhibit a linear power broadening in the small Rabi frequency regime, and becomes a highly nonlinear function of pump power in the large Rabi frequency regime [26]. Due to the resolution limit of the spectrometer, however, this broadening is difficult to resolve from the data in Fig. 2. In order to improve the spectral resolution of the measurement system we place a tunable fiber Fabry-Perot filter with 0.9 GHz bandwidth in front of the spectrometer. Measurements are performed by tuning the filter and recording the intensity, determined by integrating the signal over a 14 GHz spectral window (corresponding to five pixels of CCD) around the center frequency of the Fabry-Perot mode. We measure the linewidth of the lower energy sideband since it is always highly detuned from the cavity and therefore spectrally well separated from the background photons created by nonresonant energy transfer.

Figure 3(a) shows the measured high-resolution spectrum of the lower energy sideband for several different pump powers at a detuning of $\Delta_{cx}/2\pi = 42$ GHz. For each spectrum, the sideband linewidth is determined by fitting the measured data with two Lorentzian functions, one representing the sideband peak while the other the laser scatter. The fit is shown as a solid red line in the figure. Figure 3(b) shows the measured full-width half-maximum linewidth of the Mollow sideband as a function of $|\Omega/2\pi|^2$. Here Ω is determined by measuring the detuning of the lower energy sideband from the laser, where the sideband center frequency is obtained from the Lorentzian fit. In the small Rabi frequency regime ($\Omega < \Delta_{cx}$) we observe a linear increase in the sideband linewidth as a function of pump power (proportional to $|\Omega|^2$). At a pump power of $|\Omega/2\pi|^2 = 2040$ GHz^2 (denoted by the dashed vertical line), the higher energy sideband becomes resonant with the cavity and the system transitions to the large Rabi frequency regime ($\Omega > \Delta_{cx}$). At this point the linewidth exhibits a very different broadening behavior where it becomes a highly nonlinear function of pump power. In

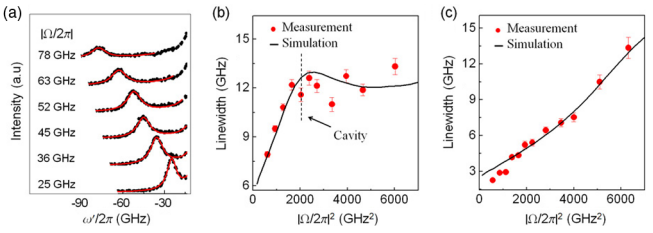

FIG. 3 (color online). (a) High spectral resolution measurement (black circles) of the lower energy sidebands using the Fabry-Perot filter for $\Delta_{cx}/2\pi = 42$ GHz. Red curves show the Lorentzian fit. Remaining panels show the measured and numerically calculated linewidths for (b) $\Delta_{cx}/2\pi = 42$ GHz and (c) $\Delta_{cx}/2\pi = 85$ GHz.

the large Rabi frequency regime, the linewidth is largely insensitive to the pump power. We observe the transition between these two behaviors precisely at the point where the higher energy sideband crosses the cavity mode. In contrast, Fig. 3(c) shows the lower energy sideband linewidths obtained for a larger quantum dot-cavity detuning ($\Delta_{cx}/2\pi = 85$ GHz) where the system remains in the small Rabi frequency regime. Here, the linewidth shows nearly linear increase over the same range of excitation power.

To gain further insight into the mechanism for the nonlinear power broadening behavior we perform numerical calculations of the master equation $\dot{\rho} = -i/\hbar[\mathbf{H}, \rho] + \mathbf{L}\rho$, where ρ is the density matrix of the system. The system Hamiltonian is given by

$$\mathbf{H} = \hbar\Delta_c \mathbf{a}^\dagger \mathbf{a} + \hbar\Delta_x \sigma_\mathbf{z}/2 + \hbar g(\sigma_+ \mathbf{a} + \mathbf{a}^\dagger \sigma_-) + \hbar\sqrt{\kappa} J(\mathbf{a} + \mathbf{a}^\dagger). \quad (1)$$

In Eq. (1), $\Delta_c = \omega_c - \omega_L$ and $\Delta_x = \omega_x - \omega_L$. In addition, $\sigma_\mathbf{z}$ is the population difference operator between the excited and ground state of the quantum dot, σ_- (σ_+) represents the dipole lowering (raising) operator for the quantum dot, $\mathbf{a}$ ($\mathbf{a}^\dagger$) is the cavity photon annihilation (creation) operator, and $J = \sqrt{\eta P/\hbar\omega}$ is the driving field amplitude. The Liouvillian superoperator $\mathbf{L}$ accounts for all nonunitary Markovian processes including cavity and quantum dot damping, pure dephasing, and phonon-mediated energy transfer. This operator can be written as

$$\mathbf{L} = \gamma\mathcal{D}(\sigma_-) + \kappa\mathcal{D}(a) + \gamma_d\mathcal{D}(\sigma_+\sigma_-) + \gamma_{ph}^{a^\dagger\sigma_-}\mathcal{D}(a^\dagger\sigma_-) + \gamma_{ph}^{a\sigma_+}\mathcal{D}(a\sigma_+), \quad (2)$$

where $\mathcal{D}(\mathcal{C})\rho = \mathcal{C}\rho\mathcal{C}^\dagger - 1/2\mathcal{C}^\dagger\mathcal{C}\rho - 1/2\rho\mathcal{C}^\dagger\mathcal{C}$ is a general Linblad operator form for the collapse operator $\mathcal{C}$. In Eq. (2), γ is the quantum dot spontaneous emission rate, κ is the cavity energy decay rate, and γ_d is the quantum dot pure dephasing rate. To account for the phonon-mediated dephasing, we adopt the formalism of Ref. [23] and include the last two Linblad terms where we define $\gamma_{ph}^{a^\dagger\sigma_-}$ and $\gamma_{ph}^{a\sigma_+}$ as the phonon-mediated dephasing rates; physically these processes describe the destruction of a cavity photon leading to the creation of an exciton or vice versa.

We perform all numerical calculations using an open source quantum optics toolbox [35]. We calculate the two-time covariance function $\langle \mathbf{a}^\dagger(t+\tau), \mathbf{a}(t)\rangle$ in the steady state limit using quantum regression theory. The power spectrum is obtained by taking the Fourier transform of the covariance function. We set the cavity decay rate and the quantum dot-cavity coupling strength to the measured values of $\kappa/2\pi = 36$ GHz and $g/2\pi = 15.3$ GHz, respectively. The spontaneous emission rate is $\gamma/2\pi = 0.16$ GHz and the pure dephasing rate is $\gamma_d/2\pi = 1$ GHz [36].

The sideband linewidth is obtained by fitting the calculated power spectrum with a Lorentzian at each Rabi frequency. We determine $\gamma_{ph}^{a^\dagger\sigma_-}$ and $\gamma_{ph}^{a\sigma_+}$ in this calculation by treating them as fitting parameters and performing a linear least squares optimization. From the fit we obtain $\gamma_{ph}^{a^\dagger\sigma_-}/2\pi = 0.19(\pm 0.03)$ GHz and $\gamma_{ph}^{a\sigma_+}/2\pi = 0.28(\pm 0.05)$ GHz. These phonon dephasing rates are consistent with the previously predicted values [23,26]. The difference between $\gamma_{ph}^{a^\dagger\sigma_-}$ and $\gamma_{ph}^{a\sigma_+}$ is due to the fact that when the cavity is blue-detuned from the quantum dot, the phonon dephasing process related to $\gamma_{ph}^{a^\dagger\sigma_-}$ requires a phonon absorption while the reverse process denoted by $\gamma_{ph}^{a\sigma_+}$ does not. The solid line in Fig. 3(b) shows the theoretically calculated linewidths of the lower energy sideband as a function of $|\Omega/2\pi|^2$ for $\Delta_{cx}/2\pi = 42$ GHz. The calculations exhibit good agreement with the measurement results and predict nonlinear power broadening when the sideband is resonant with the cavity. We attribute the small mismatch between measured data and calculations at large Rabi frequencies to sample drift and misalignment during the measurement process. This drift induces a fluctuating coupling efficiency that can perturb both the center frequency and linewidth of the sideband emission. Figure 3(c) plots the same calculations for $\Delta_{cx}/2\pi = 85$ GHz. Here we obtain phonon coupling rates of $\gamma_{ph}^{a^\dagger\sigma_-}/2\pi = 0.17(\pm 0.02)$ GHz and $\gamma_{ph}^{a\sigma_+}/2\pi = 0.37(\pm 0.04)$ GHz. These values are different from those determined in the fit to Fig. 3(b) because both the phonon density of states and phonon occupation probabilities depend on the phonon energy, which increases with cavity detuning [22,23].

To explain the cause of nonlinear power broadening, we consider the situation where there is no phonon-mediated energy transfer or pure dephasing by setting $\gamma_{ph}^{a^\dagger\sigma_-} = \gamma_{ph}^{a\sigma_+} = \gamma_d = 0$. The blue dotted line in Fig. 4(a) shows the calculated results for this condition where the detuning is set to $\Delta_{cx}/2\pi = 42$ GHz. In this case the only interaction between the quantum dot and cavity is through the coherent Jaynes-Cummings term in the Hamiltonian. The sideband linewidth exhibits a resonant behavior that peaks when

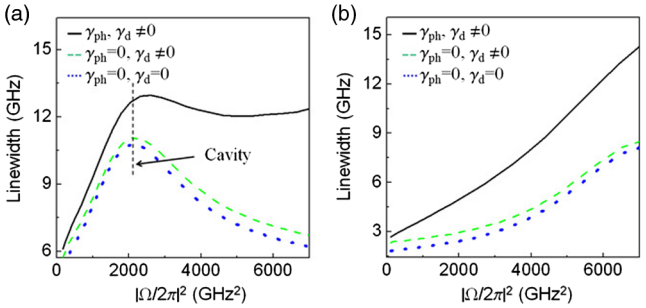

FIG. 4 (color online). (a) Numerically calculated linewidths for $\Delta_{cx}/2\pi = 42$ GHz. Blue dotted line: calculated linewidth with no phonon coupling or pure dephasing, green dashed line: calculated linewidth with pure dephasing but no phonon coupling, black solid line: both phonon coupling and pure dephasing included. (b) Same as panel a, but for $\Delta_{cx}/2\pi = 85$ GHz.

the higher energy sideband is on-resonance with the cavity. The green dashed line shows the situation where we have included pure dephasing, which does not change the resonant behavior but simply broadens the sideband linewidth independent of the excitation power. The model consisting of only a unitary Jaynes-Cummings interaction and pure dephasing exhibits poor agreement with the experimental results. When we add the phonon-mediated dephasing terms (black solid line) we obtain a significantly better agreement with the measured data. Figure 4(b) plots the same calculations for a detuning of $\Delta_{cx}/2\pi = 85$ GHz. In this case we do not predict a nonlinear power broadening because we are always in the small Rabi frequency regime. Nevertheless, without the phonon term the calculations predict a much smaller power induced broadening than what is observed experimentally.

These calculations provide an explanation for the nonlinear power dependence of the linewidth. Away from resonance, phonon coupling is the dominant broadening mechanism and results in a monotonic increase of the sideband linewidth as a function of pump power. Near resonance, however, the coherent Jaynes-Cummings term significantly contributes to the sideband linewidth [Fig. 4(a)]. In the small Rabi frequency regime, both phonon-mediated dephasing and coherent Jaynes-Cummings interaction exhibit an increase in linewidth as a function of pump power and therefore constructively add. In the large Rabi frequency regime, the Jaynes-Cummings term exhibits a decrease in the linewidth as a function of pump power. Instead of adding to the linewidth, this decrease now partially cancels out the monotonic increase due to phonon coupling. The interplay between these two terms therefore leads to the nonlinear power dependence of the linewidth broadening observed in the experimental measurements.

In conclusion, we have demonstrated that the Mollow triplet spectrum exhibits both a large asymmetry and excitation induced dephasing with a nonlinear power dependence. Our experimental results agree well with recent theoretical prediction and provide further insight into the Mollow triplet emission properties in the large Rabi frequency regime. These results could find important applications for single and heralded photon sources with large frequency tunability [17]. They could also provide a direct pathway for achieving population inversion with a strongly driven single emitter [18].

We would like to acknowledge S. Hughes for helpful discussions. This work was supported by the ARO MURI on hybrid quantum interactions (Grant No. W911NF09104), the Physics Frontier Center at the Joint Quantum Institute, a DARPA Defense Science Office grant (Grant No. W31P4Q0910013), and the ONR Applied Electromagnetics Center. E. W. would like to acknowledge support from an NSF CAREER award (Grant No. ECCS. 0846494) and a DARPA Young Faculty Award (Grant No. N660011114121).

*edowaks@umd.edu

[1] Th. Sauter, W. Neuhauser, R. Blatt, and P. E. Toschek, Phys. Rev. Lett. **57**, 1696 (1986).
[2] J. C. Bergquist, R. G. Hulet, W. M. Itano, and D. J. Wineland, Phys. Rev. Lett. **57**, 1699 (1986).
[3] A. N. Vamivakas, C.-Y. Lu, C. Matthiesen, Y. Zhao, S. Falt, A. Badolato, and M. Atatüre, Nature (London) **467**, 297 (2010).
[4] H. J. Kimble, M. Dagenais, and L. Mandel, Phys. Rev. Lett. **39**, 691 (1977).
[5] C. Matthiesen, A. N. Vamivakas, and M. Atatüre, Phys. Rev. Lett. **108**, 093602 (2012).
[6] C. Matthiesen, M. Geller, C. H. H. Schulte, C. Le Gall, J. Hansom, Z. Li, M. Hugues, E. Clarke, and M. Atatüre, Nat. Commun. **4**, 1600 (2013).
[7] L. Childress, J. M. Taylor, A. S. Sörensen, and M. D. Lukin, Phys. Rev. Lett. **96**, 070504 (2006).
[8] L.-M. Duan, M. J. Madsen, D. L. Moehring, P. Maunz, R. N. Kohn, and C. Monroe, Phys. Rev. A **73**, 062324 (2006).
[9] B. R. Mollow, Phys. Rev. **188**, 1969 (1969).
[10] F. Schuda, C. R. Stroud, Jr, and M. Hercher, J. Phys. B **7**, L198 (1974).
[11] A. Muller, E. B. Flagg, P. Bianucci, X. Y. Wang, D. G. Deppe, W. Ma, J. Zhang, G. J. Salamo, M. Xiao, and C. K. Shih, Phys. Rev. Lett. **99**, 187402 (2007).
[12] X. Xu, B. Sun, P. R. Berman, D. G. Steel, A. S. Bracker, D. Gammon, and L. J. Sham, Science **317**, 929 (2007).
[13] A. Muller, W. Fang, J. Lawall, and G. S. Solomon, Phys. Rev. Lett. **101**, 027401 (2008).
[14] A. N. Vamivakas, Y. Zhao, C.-Y. Lu, and M. Atatüre, Nat. Phys. **5**, 198 (2009).
[15] E. B. Flagg, A. Muller, J. M. Robertson, S. Founta, D. G. Deppe, M. Xiao, W. Ma, G. J. Salamo, and C. K. Shih, Nat. Phys. **5**, 203 (2009).
[16] S. Ates, S. M. Ulrich, S. Reitzenstein, A. Löffler, A. Forchel, and P. Michler, Phys. Rev. Lett. **103**, 167402 (2009).
[17] A. Ulhaq, S. Weiler, S. M. Ulrich, R. Roßbach, M. Jetter, and P. Michler, Nat. Photonics **6**, 238 (2012).
[18] T. Quang and H. Freedhoff, Phys. Rev. A **47**, 2285 (1993).
[19] S. M. Ulrich, S. Ates, S. Reitzenstein, A. Löffler, A. Forchel, and P. Michler, Phys. Rev. Lett. **106**, 247402 (2011).
[20] A. Majumdar, A. Papageorge, E. D. Kim, M. Bajcsy, H. Kim, P. Petroff, and J. Vučković, Phys. Rev. B **84**, 085310 (2011).
[21] C. Roy and S. Hughes, Phys. Rev. Lett. **106**, 247403 (2011).
[22] A. Majumdar, E. D. Kim, Y. Gong, M. Bajcsy, and J. Vučković, Phys. Rev. B **84**, 085309 (2011).
[23] C. Roy and S. Hughes, Phys. Rev. X **1**, 021009 (2011).
[24] Y. Zhu, A. Lezama, T. W. Mossberg, and M. Lewenstein, Phys. Rev. Lett. **61**, 1946 (1988).
[25] A. Lezama, Y. Zhu, S. Morin, and T. W. Mossberg, Phys. Rev. A **39**, 2754 (1989).
[26] C. Roy, H. Kim, E. Waks, and S. Hughes, Photon Nanostruct: Fundam Appl, http://dx.doi.org/10.1016/j.photonics.2012.05.004 (2012).
[27] Y. Akahane, T. Asano, B.-S. Song, and S. Noda, Opt. Express **13**, 1202 (2005).
[28] S. Ates, S. M. Ulrich, A. Ulhaq, S. Reitzenstein, A. Löffler, S. Höfling, A. Forchel, and P. Michler, Nat. Photonics **3**, 724 (2009).

[29] M. Winger, T. Volz, G. Tarel, S. Portolan, A. Badolato, K. J. Hennessy, E. L. Hu, A. Beveratos, J. Finley, V. Savona *et al.*, Phys. Rev. Lett. **103**, 207403 (2009).
[30] D. Englund, A. Majumdar, A. Faraon, M. Toishi, N. Stoltz, P. Petroff, and J. Vučković, Phys. Rev. Lett. **104**, 073904 (2010).
[31] U. Hohenester, Phys. Rev. B **81**, 155303 (2010).
[32] S. Hughes, P. Yao, F. Milde, A. Knorr, D. Dalacu, K. Mnaymneh, V. Sazonova, P. J. Poole, G. C. Aers, J. Lapointe *et al.*, Phys. Rev. B **83**, 165313 (2011).
[33] S. Mosor, J. Hendrickson, B. C. Richards, J. Sweet, G. Khitrova, H. M. Gibbs, T. Yoshie, A. Scherer, O. B. Shchekin, and D. G. Deppe, Appl. Phys. Lett. **87**, 141105 (2005).
[34] S. Strauf, M. T. Rakher, I. Carmeli, K. Hennessy, C. Meier, A. Badolato, M. J. A. Dedood, P. M. Petroff, E. L. Hu, E. G. Gwinn *et al.*, Appl. Phys. Lett. **88**, 043116 (2006).
[35] S. M. Tan, J. Opt. B **1**, 424 (1999).
[36] I. Favero, A. Berthelot, G. Cassabois, C. Voisin, C. Delalande, P. Roussignol, R. Ferreira, and J. M. Gérard, Phys. Rev. B **75**, 073308 (2007).